Aptamers as Affinity Reagents in an Integrated Electrophoretic Lab-on-a-Chip Platform

ARTICLE *in* ANALYTICAL CHEMISTRY · OCTOBER 2010

Impact Factor: 5.64 · DOI: 10.1021/ac101106m · Source: PubMed

6 AUTHORS, INCLUDING:

Xianbin Yang
A M Biotechnologies LLC
34 PUBLICATIONS **369** CITATIONS
SEE PROFILE

Anup K Singh
Sandia National Laboratories
150 PUBLICATIONS **3,805** CITATIONS
SEE PROFILE

Anal. Chem. **2010,** *82,* 8813–8820

Aptamers as Affinity Reagents in an Integrated Electrophoretic Lab-on-a-Chip Platform

Ariel H. Hecht,[†,‡] Greg J. Sommer,[†] Ross H. Durland,[§] Xianbin Yang,[§] Anup K. Singh,[†] and Anson V. Hatch*[,†]

Sandia National Laboratories, Livermore, California 94551, United States, University of Michigan, Ann Arbor, Michigan 48109, United States, and AM Biotechnologies, LLC, Houston, Texas 77034, United States

Nucleic acid based affinity reagents (e.g., aptamers) offer several possible advantages over antibodies as specific recognition elements in biochemical assays. Besides offering improved cost and stability, aptamers are ideal for rapid electrophoretic analysis due to their low molecular weight and high negative charge. While aptamers have proven well-suited for affinity-shift electrophoretic analysis, demonstrating a fully integrated aptamer-based assay platform represents an important achievement toward low-cost point-of-care analysis, particularly for remote or resource poor settings where cost and ambient stability of reagents is a key consideration. Here we perform and evaluate the suitability of aptamer-based affinity assays for two clinically relevant target analytes (IgE using a known aptamer and NF-κB using a thio-modified aptamer) in an integrated electrophoretic gel-shift platform. Key steps of (i) mixing sample with aptamer, (ii) buffer exchange, and (iii) preconcentration of sample were successfully integrated on-chip upstream of a fluorescence-based gel-shift analysis step. This approach, utilizing a size-exclusion membrane optimized here for aptamer retention and preconcentration with sample, enables automated sample-to-answer for trace analytes in 10 min or less. We addressed notable non-specific interference from serum proteins by adding similar nucleic acid competitors to suppress such interactions with the aptamer. Nanomolar sensitivities were demonstrated and integrated preconcentration of sample provides an important means of further improving detection sensitivities. Aptamers proved superior in many respects to antibody reagents, particularly with regard to speed and resolution of gel-shifts associated with specific binding to target.

Over the past few decades, microfluidic devices have garnered much attention as potential medical diagnostic tools. Such devices are particularly attractive for satisfying diagnostic needs at the point-of-care or first responder settings without phlebotomy through a high level of automation in a compact device that requires only a droplet of sample.[1−4] Advantages of scale and integration with these devices also tend to shorten analysis times from hours to minutes, while still achieving quantitative detection of trace analytes. Our group at Sandia has developed an integrated microfluidic platform that addresses several requirements for point-of-care diagnostics of disease and toxin exposure.[5−10] To date we have reported on diagnostic assays that utilize antibodies as specific recognition elements, as is typical for the majority of commercial diagnostics targeting proteins and several other classes of biomarkers. However for certain point-of-care settings and first responder scenarios, cost and logistical concerns related to stability and shelf life of antibodies warrant consideration of alternative affinity reagents. Several promising antibody alternatives have been developed for therapeutic and diagnostic purposes over the last couple of decades with an emphasis on engineered polypeptide and polynucleotide affinity reagents.[11−13] These reagents can be engineered with high affinity, specificity, and thermostability and are manufacturable in high purity and reproducibility at low cost once identified.

Aptamers are selected from randomized nucleotide sequence pools to bind to a molecular target (e.g., proteins or peptides) with high affinity and specificity, similar to antibodies.[14] Aptamers have been used for a wide range of diagnostic[15−19] and therapeu-

* To whom correspondence should be addressed. P.O. Box 969 MS 9291 Livermore, CA 94550. Phone: 929-294-2692. E-mail: ahatch@sandia.gov.

† Sandia National Laboratories.

‡ University of Michigan.

§ AM Biotechnologies, LLC.

(1) Jokerst, J. V.; Floriano, P. N.; Christodoulides, N.; Simmons, G. W.; McDevitt, J. T. *Lab Chip* **2008**, *8*, 2079–2090.
(2) Kamholz, A. E.; Weigl, B. H.; Finlayson, B. A.; Yager, P. *Anal. Chem.* **1999**, *71*, 5340–5347.
(3) Lee, H.; Sun, E.; Ham, D.; Weissleder, R. *Nat. Med.* **2006**, *14*, 869–874.
(4) Sia, S.; Kricka, L. *Lab Chip* **2008**, *8*, 1982–1983.
(5) Herr, A. E.; Hatch, A. V.; Throckmorton, D. J.; Tran, H. M.; Brennan, J. S.; Giannobile, W. V.; Singh, A. K. *Proc. Natl. Acad. Sci. U.S.A.* **2007**, *104*, 5268–5273.
(6) Hatch, A. V.; Herr, A. E.; Throckmorton, D. J.; Brennan, J. S.; Singh, A. K. *Anal. Chem.* **2006**, *78*, 4976–4984.
(7) Herr, A. E.; Singh, A. K. *Anal. Chem.* **2004**, *76*, 4727–4733.
(8) Herr, A. E.; Throckmorton, D. J.; Davenport, A. A.; Singh, A. K. *Anal. Chem.* **2005**, *77*, 585–590.
(9) Meagher, R. J.; Hatch, A. V.; Renzi, R. F.; Singh, A. K. *Lab Chip* **2008**, *8*, 2046–2053.
(10) Renzi, R. F.; Stamps, J.; Horn, B. A.; Ferko, S.; VanderNoot, V. A.; West, J. A.; Crocker, R.; Wiedenman, B.; Yee, D.; Fruetel, J. A. *Anal. Chem.* **2005**, *77*, 435.
(11) Boschek, C. B.; Apiyo, D. O.; Soares, T. A.; Engelmann, H. E.; Pefaur, N. B.; Straatsma, T. P.; Baird, C. L. *Protein Eng., Des. Sel.* **2009**, *22*, 325–332.
(12) Ligler, F. S., Taitt, C. R., Eds.; *Optical Biosensors: Today and Tomorrow*, 2nd ed.; Elsevier: Amsterdam, The Netherlands, 2008.
(13) Brody, E. N.; Gold, L. *Rev. Mol. Biotechnol.* **2000**, *74*, 5–13.
(14) Klussmann, S., Ed.; *The Aptamer Handbook: Functional Oligonucleotides and Their Applications*; Wiley-VCH: Weinheim, Germany, 2006.
(15) Ellington, A. D.; Szostak, J. W. *Nature* **1990**, *346*, 818–822.

10.1021/ac101106m
Published on Web 10/14/2010

tic[20] applications. Most aptamers to date have been derived through the SELEX process (systematic evolution of ligands by exponential enrichment), whereby a randomly generated pool of oligonucleotides is mixed with the target of interest and oligonucleotides that display affinity for the target are separated and amplified repeatedly until the highest affinity oligonucleotides are isolated.[15] Recently, an alternative process in which the pool of oligonucleotides is synthesized on beads has emerged which reduces the need for multiple enrichment cycles and better accommodates nucleotide modifications. The target is mixed with the beads, and beads displaying affinity for the target are isolated and the corresponding sequences are identified. One or a few rounds of this process can yield a sequence with high affinity for the target.[21−26] Incorporating modified nucleotides can improve nuclease resistance and enrich the chemical complexity of the library to enhance affinity and specificity. A prominent example is the thioaptamer, incorporating phosphorothioate-modifications in which one (monothio) or both (dithio) of the nonbridging oxygen atoms on the phosphate backbone of the nucleic acid strand are replaced with sulfur atoms.[24,26]

Aptamers exhibit several benefits over antibodies for diagnostic applications. Aptamers can be synthesized to target diverse classes of molecules, precisely controlled for desired physicochemical properties, easily modified for purposes such as labeling, and produced at low cost with high uniformity from batch to batch. Aptamers are also significantly more robust than antibodies,[27] making them better suited for ambient reagent storage and point-of-care operation and eliminating cold-chain transportation needs. This property is especially advantageous for devices designed for operation in resource-deficient areas, such as third-world regions and outer space.

Here, we demonstrate the suitability of nucleic acid affinity reagents in an integrated electrophoretic gel-shift detection platform. A model aptamer[28] targeting immunoglobulin E (IgE) and a model thioaptamer[29,30] targeting nuclear factor-κB (NF-κB) were evaluated. IgE is one of five classes of antibodies produced by humans and functions primarily in generating allergic reactions[31] and in defending the body against parasites.[32] NF-κB is a protein that controls the transcription of DNA and mediates a wide range of physiological responses, specifically immune responses to cytokines and antigens.[33,34] Improper regulation of NF-κB can lead to a variety of diseases, including cancer.[35,36]

We investigated assay performance with spiked serum samples where potential interference from the serum matrix and high-abundance proteins on affinity shift assays have been explored to a limited extent with conflicting results. Some previous experiments have reported significant nonspecific interactions between DNA aptamers and serum proteins in 10% serum,[37] in cell culture media,[38] as well as the benefits of using an excess of nonspecific aptamers to minimize interactions between serum proteins and aptamers in capillary electrophoresis[39] and fluorescence detection.[40] Others have reported serum-based aptamer assays without notable interference in capillary electrophoresis[41] and fluorescence polarization anisotropy.[18] Here, a competitive inhibition strategy using excess nonspecific oligonucleotides was required to suppress serum interference.

Finally, a distinguishing feature of the integrated platform is the incorporation of a size-exclusion membrane to mix and incubate affinity reagents with sample proteins as well as to preconcentrate sample proteins and perform sample buffer exchange prior to electrophoretic separations analysis.[5,6,9] This mode of mixing reagents automates key assay steps on-chip in rapid fashion. Enhancing the assay sensitivity by several orders of magnitude through preconcentration is critical for achieving required detection limits for a number of trace analytes. However, the membrane formulations previously reported for this platform[5,6] were optimized for concentrating SDS denatured proteins prior to SDS PAGE sizing and for trapping antibody reagents and target proteins prior to gel-shift affinity assays. We report on system performance with aptamer reagents of smaller size and higher charge density. A key benefit of employing aptamers is their superior gel shift properties compared to antibodies. Modification and optimization of the exclusion membrane were required to improve the performance of integrated aptamer-based affinity assays. Best results were achieved through incorporation of a mild charge into the nanoporous size exclusion membrane. We demonstrate that on-chip preconcentration, mixing, buffer exchange, and detection of target analytes in serum samples are readily achieved within the integrated platform.

(16) Li, Y.; Guo, L.; Zhang, F.; Tang, J.; Xie, J. *Electrophoresis* **2008**, *29*, 2570–2577.
(17) Ferapontova, E. E.; Olsen, E. M.; Gothelf, K. V. *J. Am. Chem. Soc.* **2008**, *130*, 4256–4258.
(18) McCauley, T. G.; Hamaguchi, N.; Stanton, M. *Anal. Biochem.* **2003**, *319*, 244–250.
(19) Lai, R. Y.; Plaxco, K. M.; Heeger, A. J. *Anal. Chem.* **2007**, *79*, 229–233.
(20) Fine, S. L.; Martin, D. F.; Kirkpatrick, P. *Nat. Rev. Drug Discovery* **2005**, *4*, 187–188.
(21) Leary, J. F.; Reece, L. M.; Yang, X.; Gorenstein, D. G. *Proc. Soc. Photo-Opt. Instr. Eng* **2005**, 216–223.
(22) Yang, X.; Gorenstein, D. G. *Curr. Drug Targets* **2004**, *5*, 705–15.
(23) Yang, X.; Li, X.; Prow, T. W.; Reece, L. M.; Bassett, S. E.; Luxon, B. A.; Herzog, N. K.; Aronson, J.; Shope, R. E.; Leary, J. F.; Gorenstein, D. G. *Nucleic Acids Res.* **2003**, *31*, e54.
(24) Bassett, S. E.; Fennewald, S. M.; King, D. J.; Li, X.; Herzog, N. K.; Shope, R.; Aronson, J. F.; Luxon, B. A.; Gorenstein, D. G. *Biochemistry* **2004**, *43*, 9105–9115.
(25) Yang, X.; Bassett, S. E.; Li, X.; Luxon, B. A.; Herzog, N. K.; Shope, R. E.; Aronson, J.; Prow, T. W.; Leary, J. F.; Kirby, R.; Ellington, A. D.; Gorenstein, D. G. *Nucleic Acids Res.* **2002**, *30*.
(26) King, D. J.; Bassett, S. E.; Li, X.; Fennewald, S. A.; Herzog, N. K.; Luxon, B. A.; Shope, R.; Gorenstein, D. G. *Biochemistry* **2002**, *41*, 9696–9706.
(27) Jayasena, S. D. *Clin. Chem.* **1999**, *45*, 1628–1650.
(28) Wiegand, T. W.; Williams, P. B.; Dreskin, S. C.; Jouvin, M.-H.; Kinet, J.-P.; Tasset, D. *J. Immunol.* **1996**, *157*, 221–230.
(29) Volk, D. E.; Yang, X.; Fennewald, S. M.; King, D. J.; Bassett, S. E.; Venkitachalam, S.; Herzog, N.; Luxon, B. A.; Gorenstein, D. G. *Bioorg. Chem.* **2002**, *30*, 396–419.
(30) Yang, X. B.; Fennewald, S.; Luxon, B. A.; Aronson, J.; Herzog, N. K.; Gorenstein, D. G. *Bioorg. Med. Chem. Lett.* **1999**, *9*, 3357–3362.
(31) Gould, H. J.; Sutton, B. J.; Beavil, A. J.; Beavil, R. L.; McCloskey, N.; Coker, H. A.; Fear, D.; Smurthwaite, L. *Annu. Rev. Immunol.* **2003**, *21*, 579–628.
(32) Sutton, B. J.; Gould, H. J. *Nature* **1993**, *366*, 421–428.
(33) Baldwin, A. S. *Annu. Rev. Immunol.* **1996**, *14*, 649–683.
(34) Gilmore, T. D. *Oncogene* **1999**, *18*, 6842–6844.
(35) Dolcet, X.; Llobet, D.; Pallares, J.; Matias-Guiu, X. *Virchows Arch.* **2005**, *446*, 475–482.
(36) Mann, D. A.; Oakley, F. *J. Hepatol.* **2005**, *42*.
(37) Fischer, N. O.; Tarasow, T. M.; Tok, J. B. H. *Anal. Biochem.* **2008**, *373*, 121–128.
(38) Pavski, V.; Le, X. C. *Anal. Chem.* **2001**, *73*, 6070–6076.
(39) Zhang, H.; Li, X.-F.; Le, X. C. *J. Am. Chem. Soc.* **2007**, *130*, 34–35.
(40) Tang, J.; Yu, T.; Guo, L.; Xie, J.; Shao, N.; He, Z. *Biosens. Bioelectron.* **2007**, *22*, 2456–2463.
(41) Haes, A. J.; Giordano, B. C.; Collins, G. E. *Anal. Chem.* **2006**, *78*, 3758–3764.
(42) German, I.; Buchanan, D.; Kennedy, R. *Anal. Chem.* **1998**, *70*, 4540–4545.

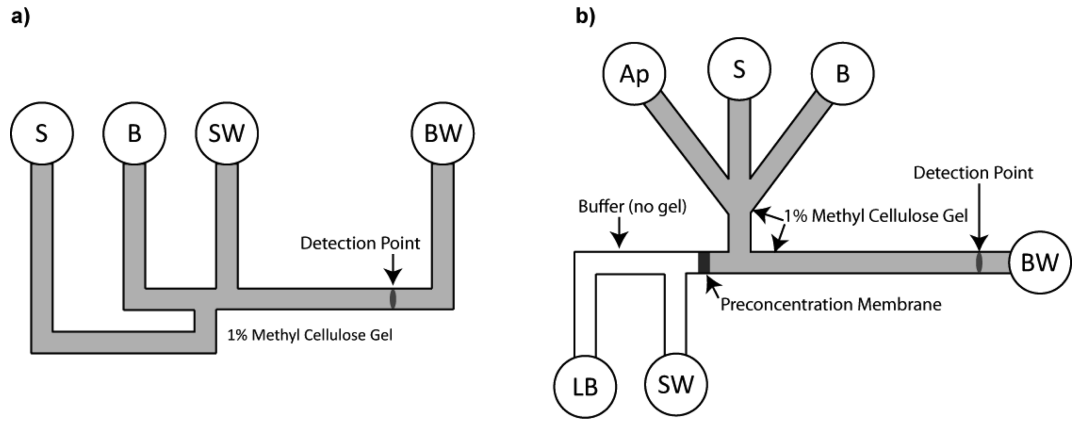

Figure 1. Schematics of offset T-chip and preconcentration chip designs. (a) Offset T-chip: S = sample inlet, B = buffer inlet, SW = sample waste outlet, and BW = buffer waste outlet. Approximate length from junction to BW is 2.9 cm. Detector is positioned approximately 15 mm from the junction. (b) Preconcentration chip: Ap = aptamer inlet, S = sample inlet, B = buffer inlet, LB = loading buffer, SW = sample waste, BW = buffer waste outlet. The detector is positioned approximately 15 mm from membrane. All channels are 100 μm wide $\times$ 35 μm deep. The voltage schemes for conducting the assays are included in the Methods and Materials section.

METHODS AND MATERIALS

Reagents. Human IgE protein (MW 190 kDa) was obtained from Scripps Laboratories (San Diego, CA). Human Recombinant NF-κB (p50, 50 gsu) was obtained from the Promega Corporation (Madison, WI). AlexaFluor 488- and 647-labeled anti-IgE aptamer[28] (MW 13.2 kDa) was obtained from Integrated DNA Technologies (Coralville, IA). The sequences for these aptamers are shown below with * denoting Alexa Fluor dye.

5′-*TTTGGGGCACGTTTATCCGTCCCTAGTGGCGTGCCCC-3′

AlexaFluor 647-labeled anti-NF-κB p50 mouse monoclonal antibody was purchased from Santa Cruz Biotechnology (Santa Cruz, CA). AlexaFluor 647-labeled anti-NF-κB thioaptamer (MW ~10.2 kDa) was obtained from AM Biotechnologies (Houston, TX). Bold and underlined bases represent phosphorodithioate modifications.

5′- AF647-CCAGGAGA**TT**CCAC - 3′
3′- G**G**TC**C**T**C**TAAG**G**AC - 5′

Masking aptamers, AB77A (MW 17.2 kDa) and AB77B (MW 17.3 kDa), synthetic oligonucleotides with 5′ biotin, were also obtained from AM Biotechnologies (Houston, TX).

AB77A: 5′-biotin-
CATCCCTCTGTC**A**ATACCG**A**ACACAAA**A**GGG**A**AAA**A**GCCC**A**CCCATCGCCTTGAA-3′
AB77B: 5′-biotin-
CAACCATGGATTAGC**A**CTCC**A**GG**A**TGG**A**GCGCCCCG**A**CTG**A**TCTTGCCGCCCAA-3′

3-(Trimethoxysilyl)propyl methacrylate (98%), 40% acrylamide, 30% (37.5:1) acrylamide/bisacrylamide, bovine serum albumin (BSA), sodium azide, and methyl cellulose powder were purchased from Sigma (St. Louis, MO). A fraction of BSA was labeled with AlexaFluor 647 per the manufacturer's instructions to be used as an internal standard for antibody-based immunoassays. *N*,*N*′-methylenebisacrylamide and 0.2 M p*K* 4.6 and p*K* 6.2 immobiline solutions were obtained from Fluka (Buchs, Switzerland). Water-soluble photoinitiator 2,2′-azobis[2-methyl-*N*-(2-hydroxyethyl)propionamide] (VA-086) was purchased from Wako Chemicals (Richmond, VA). Tris-glycine (10×, 25 mM Tris, 192 mM glycine, pH 8.3) electrophoresis buffer was purchased from BioRad (Hercules, CA). Deionized water (18.2 MΩ) was obtained using an Ultrapure water system from Millipore (Milford, MA). Off the clot mouse serum was purchased from Innovative Research (Novi, MI). Upon receipt, serum was thawed at 37 °C, mixed with 0.05% (w/v) sodium azide, filtered with 0.2 μm syringe filters, (Whatman, U.K.), aliquotted, and stored at −20 °C until use.

Microchip Fabrication. Glass (fused silica) microchips were designed in-house and fabricated by Caliper Life Sciences (Hopkinton, MA) using standard photolithography, wet etching, bonding, and dicing methods. Two previously described microchip designs[5,7] were used in this work: a standard offset T design (Figure 1a) and a more complex integrated preconcentration device (Figure 1b). Note that, unlike previous publications from our group, devices in this work used noncrosslinked 1% methyl cellulose (MC) solutions as the sieving media versus the in situ photopolymerized polyacrylamide used previously.[6,42] MC (1%) was found to be advantageous for the present application in terms of device yield and reusability, while providing sufficient sieving power for the analytes of interest.

For both devices, the channel walls were first coated with acrylate-terminated self-assembled monolayers as previously described.[6,8,42] Briefly, the channels were conditioned with 1 M NaOH, rinsed with deionized water, and dried thoroughly using a vacuum. A 2:3:5 (v/v/v) mixture of 3-(trimethoxysilyl) propyl methacrylate, glacial acetic acid, and deionized water was loaded into the channels. Devices were incubated with the solution for 30 min, rinsed with a 3:7 mixture of acetic acid and water, rinsed with deionized water, and thoroughly dried with a vacuum. Next, the channels of the offset T-chips were coated with a 5% linear acrylamide coating by loading in a solution of 5% acrylamide, 0.2% (w/v) VA-086 photoinitiator and exposing to a 100 W flood UV lamp for 6 min. Following exposure, excess solution was removed via vacuum and the channels were flushed twice with MeOH and stored dry until use.

For the integrated preconcentration devices, the nanoporous polyacrylamide membranes were fabricated prior to coating the devices with the 5% linear acrylamide coating. Membrane fabrication was accomplished using in situ photopolymerization techniques previously described.[5,6,9] Briefly, the devices were loaded

with a solution of acrylamide monomer, bisacrylamide cross-linker, and VA-086 photoinitiator. For neutral size-exclusion membranes, this solution was composed of 45% T and 12% C (where % T represents the total monomer mass concentration, and % C represents the mass percentage of cross-linker to total monomer). For charged membranes, this solution was composed of 40% T, 12% C, 18.4 mM p*K* 4.6 immobiline, and 1.6 mM p*K* 6.2 immobiline (solution pH = 4.4). Approximately 50 μm-wide membranes were defined in the channel by exposure to a shaped UV laser beam (355 nm frequency-tripled Nd:YAG). Following membrane polymerization, excess monomer solution was removed via vacuum and channels were rinsed twice with MeOH and filled with 5% linear acrylamide solution for coating, as was done with the offset T chips. After the photopolymerized coating, the chips were rinsed with MeOH, dried via vacuum, and stored dry until use.

Microchip Operation. 1% MC solution was prepared by slowly dissolving 1.5 g of methyl cellulose in 100 mL of 1× Tris-glycine buffer over a hot plate. The solution was then immediately chilled and stirred in an ice bath until all the MC was dissolved. Prior to use, the chips were filled with the 1% MC gel solution via capillary wicking. Previous work has demonstrated excellent resolution between free aptamer and complex peaks through capillary electrophoresis or capillary zone electrophoresis modes without the use of a sieving matrix.[16,42] However, we employ the 1% MC liquid gel here because (a) our assays are being developed for a multiplexed chip using a single matrix that must resolve some species that require sieving, and (b) we have found sieving gels more compatible with integrated preconcentration using nanoporous size-exclusion membrane. Chips were loaded into custom manifolds, as previously described.[10] Buffer solution (no MC) is continually flowed by gravity through the channels composing the backside of the nanoporous membrane in the integrated preconcentration chips to help negate any ion depletion effects on either side of the membrane. Samples (fluorescently labeled aptamer + target analyte) were mixed in 1% MC gel solutions and added to the sample reservoir on the manifold following a 10 min incubation at room temperature. For the preconcentration experiments, the aptamer and target analyte were diluted in separate solutions and loaded into corresponding reservoirs on the manifold. During all experiments, the total sample volume was held constant at 80 μL. In each sample, the concentration of aptamer was fixed at 10 nM, and the concentration of spiked target varied from 0.250−80 nM for IgE and 2−80 nM for NF-κB. Soaking the manifold in a 5 mg/mL solution of BSA between runs reduced sample adsorption to the sides of the manifold and improved signal quality.

Platinum electrodes were inserted into each fluid reservoir on the chip and connected to a programmable high-voltage power supply developed and fabricated in-house. For the offset T-chips, separation and detection was accomplished using voltage schemes consistent with earlier operation.[7] To load the sample into the main separation channel, a 300 V/cm electric field potential was applied between the S and SW reservoirs for 60 s. The voltage was then switched to electrophoretically separate the sample in the main channel by applying 300 V/cm between the B and BW reservoirs for 120 s. For the integrated preconcentration chips, samples were first loaded into the aptamer or sample (target) reservoir, then electrophoretically driven to the preconcentration membrane by applying 10 V/cm between the respective reservoir and the SW reservoir for varying time intervals. Following preconcentration, samples were eluted from the membrane into the separation channel by applying 30 V/cm between the LB and BW reservoirs for 10 s, then separated by applying 300 V/cm between the B and BW reservoirs for 120 s.

Sample migration was observed 15 mm down the separation channel using laser-induced fluorescence (LIF). Excitation light (argon ion laser, 488 and 647 nm) was frequency modulated using a mechanical chopper (220 Hz modulation) and reflected off a dichroic mirror (XF2010) through a 40× microscope objective (New Focus, Inc., San Jose, CA) that defined the detection point on the microchip. Fluorescence was detected by a Hamamatsu H5784 photomultiplier tube (PMT). The signal from the PMT was demodulated using a lock-in amplifier (Stanford Research Systems, Sunnyvale, CA), and the signal was collected using a computer via a data acquisition interface (6020E DAQPad, National Instruments, Austin, TX). Data were collected using an in-house program written in LabVIEW (National Instruments).

Quantifying Performance. Electropherogram peak areas were calculated using a program written in-house. Complex (aptamer + target) peak areas are reported as normalized complex peak area (complex peak area/[complex peak area + free aptamer peak area]). Dose−response curves were generated by measuring the respective peak areas for varying concentrations of target analyte, then fit using the four-parameter logistic model[43] in eq 1 below

$$y = d + \frac{a - d}{\left[1 + \left(\frac{x}{c}\right)^{b}\right]} \quad (1)$$

where a is the estimated response at zero concentration of the target, b is the Hill coefficient, which refers to the steepness of the sigmoidal dose−response curve and is related to the binding constant, c is the midrange concentration (C_{50}), d is the estimated response at infinite concentration, x is the target concentration, and y is the normalized complex peak area. Although a reference standard is preferred for peak normalization, several chosen reference compounds overlapped with either the free aptamer peak or the complex peak. Instead, total fluorescence of the sample was used to normalize electropherograms, which was deemed adequate for the goals of this study.

RESULTS AND DISCUSSION

Aptamer Performance in Buffer Conditions. Representative aptamer affinity gel-shift assay results for the anti-NF-κB thio-aptamer and the anti-IgE aptamer are presented in Figure 2 and Figure S1 in the Supporting Information, respectively, for a range of target analyte concentrations. The free aptamer peaks are readily baseline resolved from the aptamer−target complex peaks using 1% MC gel solution. The peak at 20 s corresponds to the free aptamer, while the peak at 60−80 s corresponds to the aptamer bound to its target. A typical dose-dependent response was observed, with the free aptamer peak decreasing and the complex peak increasing with higher target analyte concentrations.

(43) Baud, M. In *Methods of Immunological Analysis*; Masseyeff, R., Ed.; VCH Publishers, Inc.: New York, 1993; Vol. 1, pp 656−671.

(44) Hlushkou, D.; Dhopeshwarkar, R.; Crooks, R. M.; Tallarek, U. *Lab Chip* **2008**, *8*, 1153–1162.

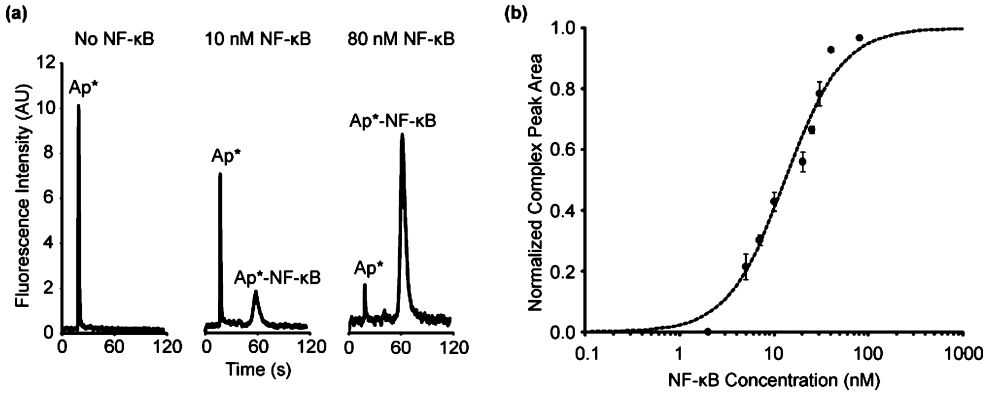

Figure 2. (a) Electropherogram of 10 nM AF647-anti-NF-κB thioaptamer with NF-κB spiked in buffer conditions. The peak at 20 s is the free aptamer peak (Ap*), and the peak around 60 s is the aptamer−target complex peak (Ap*−NF-κB). As the concentration of the target is increased (with constant aptamer concentration), the free aptamer peak decreases while the complex peak increases. (b) Dose−response curve of AF647-anti-NF-κB thioaptamer with NF-κB spiked in buffer. The curve was fit using the four-parameter logistic model in eq 1; $r^2 = 0.981$.

The dose responses plotted in Figures 2b and S1b were fit using the four-parameter logistic model in eq 1. For Figure 2b, $a = 0.00$, $b = 1.44$, $c = 13.11$, and $d = 1.00$. For Figure S1b in the Supporting Information, $a = 0.00$, $b = 1.37$, $c = 3.02$, and $d = 1.00$. The anti-IgE aptamer demonstrated dynamic sensitivity over the IgE concentration range of ~0.5−20 nM, while the anti-NF-κB thioaptamer demonstrated dynamic sensitivity over the NF-κB range of ~5−80 nM. These results are consistent with high-affinity interactions expected for these previously characterized reagents.

To demonstrate potential advantages of aptamers over antibodies for on-chip electrophoretic gel-shift detection, we compared the performance of the anti-NF-κB thioaptamer with that of an AlexaFluor 647-labeled anti-NF-κB monoclonal antibody. Free probes are separated from target-bound affinity probes based on differing electrophoretic mobilities, which are a function of the mass to charge ratio of the two species. When considering the molecular weight (MW) range of typical assay targets, MW_{target} ~ 1−200 kDa, the shift in MW upon binding in a direct assay format for aptamers ($MW_{aptamer}$ ~ 10 kDa + MW_{target}) is much greater than for standard IgG antibodies (MW_{Ab} ~ 150 kDa + MW_{target}) due to the smaller size of aptamers. Furthermore, the modest net charge density of most biochemical targets compared to the high charge density of aptamers favors enhanced mobility shifts upon binding. Gel shifts are more likely to be resolved with aptamer reagents, particularly for lower molecular weight targets including typical cytokines. The immunoassay format was first attempted using the same 1% MC gel solution used for aptamer assays; however, the sieving power of the liquid gel was not sufficient to resolve the free antibody and complex peaks. A cross-linked polyacrylamide gel 8% T, 2.6% C was therefore used to increase sieving power and achieve an immunoassay gel-shift. Electropherograms obtained with an offset T-chip are included in Figure S2 in the Supporting Information. The free antibody peak requires much longer elution time at 132 s compared to the 20 s resolution of free aptamer peaks. More importantly, the free antibody peak and the immunocomplex peak overlap significantly, preventing quantitative analysis of the electropherograms, whereas the aptamer complex is easily baseline resolved.

Although the resolution advantage of aptamers over antibodies is clearly apparent for this case by visual inspection of the electropherograms, we can also quantify the separation resolution for each case using eq 2 below

$$R_s = \frac{T_2 - T_1}{2(\tau_1 + \tau_2)} \quad (2)$$

where T_1 and T_2 represent the elution time of the free probe and probe−target complex, respectively, and τ_1 and τ_2 represent the standard deviation due to dispersion of the respective peaks. In general, $R_s > 1$ is desired, while $R_s = 1.5$ is considered baseline resolution. For the antibody-based electropherogram in Figure S2 in the Supporting Information, $R_s = 0.385$ (well below the desired resolution). For the corresponding electropherogram of 10 nM anti-NF-κB thioaptamer and 10 nM NF-κB in Figure 2a, $R_s = 4.86$ (well above baseline resolution). The resolution of a gel-shift assay is dependent on several factors including the affinity probe properties and buffer characteristics, and further development would likely yield an acceptable immunoassay for a target in this size range. However, this example highlights a clear general advantage in using aptamers to achieve separation resolution in this system.

Aptamer Performance in Serum. Running the aptamer-based affinity assays in serum presents a series of additional challenges due to sample complexity. Serum contains highly abundant proteins, most prominently immunoglobulin and albumin, in addition to high salt concentrations compared to optimal electrophoretic separation buffers. Consistent with some, but not all, earlier reported work with aptamer assays in serum, initial electrophoretic evaluations here showed significant nonspecific interactions of serum components with the aptamer. Figure 3a illustrates challenges imposed by nonspecific interference, where serum concentrations as low as 5% still caused significant loss of the free aptamer peak and introduction of multiple nonspecific complex peaks. In attempts to identify interfering serum components, the AF647-anti-NF-κB thioaptamer was incubated with an isolated mixture of the two most abundant serum proteins, mouse IgG and albumin, at approximate serum concentrations. However, no evidence of aptamer interactions with these proteins was observed (data not shown). To address nonspecific serum interference with aptamers, we evaluated a panel of additives spiked in the sample and running gel buffer, including 5 mg/mL of Tween-20, 0.1% (w/v) SDS, 10 mM Triton X-100, a high-salt

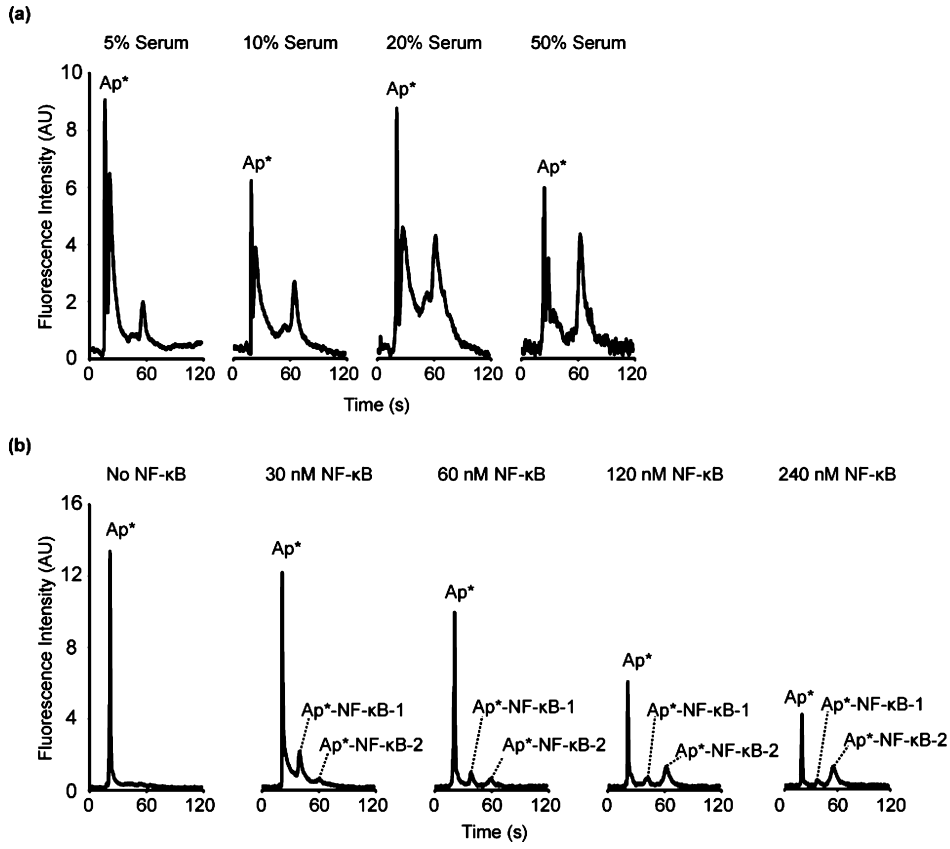

Figure 3. Comparison of assay response in serum with and without addition of a competitive suppressing agent. (a) Electropherograms of 60 nM AF647-anti-NF-κB thioaptamer incubated in 5%, 10%, 20%, and 50% serum. No NF-κB was added. The peak at 20 s represents free aptamer. Significant nonspecific serum protein interference was observed for all serum percentages in the form of multiple peaks at later time points. (b) Electropherograms of 60 nM AF647-anti-NF-κB thioaptamer with 1.2 μM of the masking aptamers suppressing nonspecific interactions in 10% serum spiked with 0, 30, 60, 120, and 240 nM NF-κB. The free aptamer peak at 20 s decreases with increasing serum concentration, as expected. Total area of complex peaks at 40 and 60 s increased with higher NF-κB concentration. The ratio of complex at 40 vs 60 s decreased with increasing analyte concentration, possibly associated with NF-κB dimerization or interaction with one or more serum components. The dose−response curve calculated from this data can be found in Figure S3 in the Supporting Information.

buffer,[42] and excesses of a 10-bp ssDNA ladder and a 100 kDa *E. coli* plasmid. However, none of these initial treatments succeeded in preventing nonspecific serum−aptamer interactions without also interfering with aptamer−target binding (not shown).

We therefore evaluated closer analogues of the anti-NF-κB thioaptamer in a competitive suppression strategy. The best success was realized using a 20-fold excess (1.2 μM) of two thioaptamer candidates similar in size and chemical properties to the anti-NF-κB thioaptamer but enriched in selection for other targets. The mixture of these masking aptamers eliminated losses of AF647-anti-NF-κB thioaptamer and the formation of nonspecific complex peaks in 10% serum (Figure 3b). Success using a similar strategy with a 40-fold excess of a nonspecific oligonucleotide was previously reported.[39,40] In our experiments, the closer analogues of the anti-NF-κB thioaptamer competed more effectively for nonspecific binding sites than small ssDNA ladder and larger plasmid DNA. Furthermore, this particular masking aptamer mixture was more effective than other masking aptamers evaluated and either masking aptamer alone (not shown). Importantly, the masking aptamers did not interfere with high-affinity binding interactions of the AF647-anti-NF-κB thioaptamer with NF-κB. These results expand upon previously described suppression strategies to mitigate matrix interference and emphasize the value in screening close analogues to aptamers under evaluation.

In contrast to the results observed in simple buffer (Figure 2), binding of AF647-anti-NF-κB thioaptamer to NF-κB in the presence of 10% serum (including the masking aptamers) resulted in two prominent complex peaks. The first complex peak decreased with increasing NF-κB concentration, while the second peak increased. Formation of higher order complexes, possibly involving one or more serum components, may explain shifts to later elution times at higher NF-κB concentrations. Further investigation is needed to elucidate this finding. A dose−response curve was approximated based on the assumption that the second and third peaks both represent the aptamer−NF-κB complex (Figure S3 in the Supporting Information). Although masking aptamers significantly reduced serum matrix interference, the dose−response was shifted by a factor of ~10 limiting detection sensitivity in comparison to buffer conditions.

Preconcentration of Aptamers Using a Charged Nanoporous Membrane. In previous work,[5,6] we have demonstrated the use of nanoporous polyacrylamide preconcentration membranes to improve the dynamic range and limit of detection of on-chip immunoassays by several orders of magnitude.[9] However, the small size of the aptamers used in this study is comparable to the MW cutoff (~10 kDa) of membranes utilized for protein preconcentration. We observed that the aptamer could be concentrated at neutral polyacrylamide membranes, but a measurable

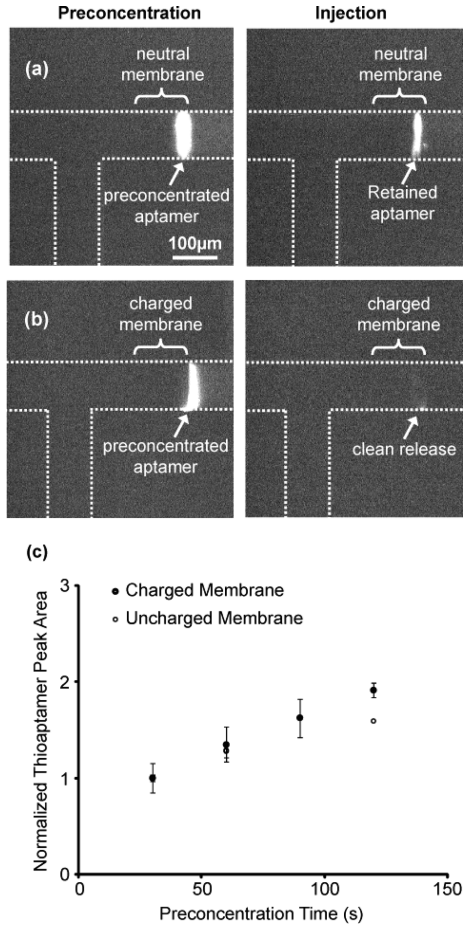

Figure 4. Comparison of neutral vs charged (pH 4.4) preconcentration membrane performance. AF647-anti-NF-κB thioaptamer aptamer loaded onto the membrane under 10 V/cm for varying preconcentration times. (a) Micrographs of loading and injection of aptamer at neutral membrane. A portion of the preconcentrated aptamer plug penetrates the neutral membrane and slowly elutes during injection, causing smearing of the injected plug. (b) Micrographs of loading and injection of aptamer at charged membrane. Compare clean release in part b with that in part a. (c) Plot of aptamer peak area following preconcentration at charged (●) vs neutral (○) membranes. Data is normalized by the 30 s preconcentration peak area. The charged membrane produces a linear concentration rate ($r^2 = 0.995$), while the neutral membrane results in a plateau in peak area with increasing preconcentration time ($r^2 = 0.862$). Error bars indicate standard deviations calculated from three separate runs.

fraction of the aptamer tends to penetrate the membrane under even very mild electric field strengths (<10 V/cm). This results in poor aptamer elution during injection to the separation channel. Aptamer penetration into a neutral membrane and losses during injection are shown in fluorescence micrographs (Figure 4a). Instead of a clean injection into the separation channel, a fraction of the concentrated aptamer plug is retained and slowly leaches from the membrane, leading to a smearing of the peak that limits separation resolution and quantitative analysis.

Hlushkou et al.[44] developed a thorough theoretical model of electrokinetic enrichment across a charged membrane. They show that the ion-permselectivity of a charged membrane leads to enhanced concentration polarization of ions across the membrane, thereby disrupting the analyte transport near the membrane. Immobilizing negatively charged constituents within preconcentration membranes has previously been shown to impact the exclusion of small analytes, and we have also found this to be true in earlier evaluations of membrane recipes for integrated electrophoretic applications involving both DNA and proteins. However, recipes have not previously been optimized to facilitate efficient transfer of electrophoretically concentrated analyte into the separation channel without peak distortion. In fact, surface immobilized charge within such membranes is known to induce concentration polarization that interferes with several aspects of preconcentration[6,44] and also subsequent transfer to a separation channel.[6] Our optimization strategy was based on formulating a high percentage polymer with a modest degree of immobilized charge to exclude DNA while minimizing the polarization expected with a highly acidic membrane. Another concern was whether low solution pH in the immediate vicinity of the membrane may interfere with aptamer/protein binding.

To control membrane acidity, dilute concentrations of acrylamido buffering compounds (immobilines) were added to the membrane monomer formulation (18.4 mM pK 4.6 immobiline, 1.6 mM pK 6.2 immobiline, total solution pH = 4.4). Experimental observation under an epi-fluorescent microscope (Figure 4b) revealed that the aptamer stacked against the negatively charged membrane without translocating across the membrane boundary and cleanly released into the separation channel with no smearing. To quantify the improvement in preconcentration efficiency with the pH 4.4 membrane in an integrated format, 10 nM AF647-anti-NF-κB thioaptamer in 1% MC was preconcentrated in chips containing both a charged and a neutral membrane. The efficiency of the pH 4.4 membrane was close to optimal based on linear increases of AF647-anti-NF-κB thioaptamer peak areas with respect to preconcentration time (Figure 4c) in contrast to an apparent plateau in preconcentration levels at higher preconcentration times with the neutral membrane. (Note that the peak areas in this figure are normalized by the peak area following 30 s of preconcentration, whereas complex peak areas in the other figures in this manuscript were normalized by the total fluorescence in the electropherogram.) Also critical for integrated preconcentration and separations based analysis is that the mildly charged membrane did not adversely impact reproducibility, peak shapes, elution times, or the linearity of enrichment with respect to preconcentration time. No concentration polarization effects were noted with the pH 4.4 membrane under the electric fields used in this work, perhaps due to the continually flowing buffer solution on the backside of the membrane. However, concentration polarization may be of issue under higher fields or longer preconcentration times. At further extremes of pH, a highly acidic membrane incorporating acrylic acid groups exhibited several symptoms associated with concentration polarization including (i) significant drops in current with similar applied electric fields, (ii) diffuse collection of labeled aptamer near the membrane during loading or preconcentration, (iii) significant smearing of aptamer during injection into the separation channel, and (iv) high run to run variability (not shown).

Integrated Mixing, Preconcentration, Incubation, and Separation. A fully integrated affinity assay combining on-chip preconcentration, mixing, incubation, and separation was demonstrated using this device incorporating membranes optimized for aptamer exclusion (Figure 5). Aptamers proved to be viable as affinity reagents for all steps of the integrated workflow.

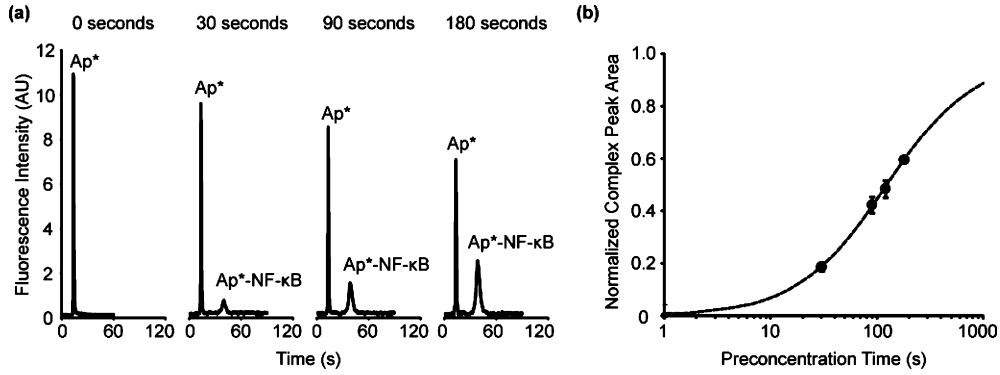

Figure 5. Integrated preconcentration and mixing of NF-κB with AF647-anti NF-κB thioaptamer at a charged nanoporous membrane. (a) Electropherograms obtained following 30 s preconcentration of 10 nM AF647-anti-NF-κB thioaptamer, followed by 0−180 s preconcentration of 20 nM NF-κB, and a 60 s buffer incubation/wash. (b) The data from part a plotted as the normalized complex peak area vs NF-κB preconcentration time. The normalized complex peak area increases sigmoidally with increasing preconcentration time, illustrating the utility of the membrane preconcentration in improving the sensitivity of the detector. Error bars indicate standard deviations calculated from three separate runs; $r^2 = 0.999$.

Fluorescent aptamer was rapidly and efficiently mixed with target sample loaded electrophoretically from separate reservoirs; representative electropherograms are shown in Figure 5a. Although the sample concentration of NF-κB was fixed at 20 nM, decreases in the free AF647-anti-NF-κB thioaptamer peak area and corresponding increases of the complex peak areas were achieved by increasing preconcentration times. Normalized complex peak areas increased sigmoidally with preconcentration times as shown in Figure 5b, indicating efficient preconcentration, mixing, and binding. Incubating reagents at the pH 4.4 membrane did not inhibit complexation of aptamer and target protein. This may occur with more acidic membranes and/or preconcentration conditions inducing significant concentration polarization, but this possibility was not further explored.

CONCLUSIONS

Aptamers are advantageous for gel shift-based lab-on-a-chip applications in point-of-care settings due to their robustness, engineered specificity, stability at a wide temperature range, and superior gel shift properties. This paper demonstrates successful use of aptamers in an integrated on-chip platform where sample can be preconcentrated, mixed with aptamer, and injected into a separation channel for quantitative gel-shift analysis. To achieve quantitative assay results in serum, we also demonstrated significant mitigation of nonspecific interference effects between the thioaptamer and serum components by adding an excess of nonspecific oligonucleotides to the sample and running gel solutions. Similarity of the suppressing oligonucleotides to the thioaptamer was important in successful mitigation of nonspecific interference.

This work also presents a basis for optimizing preconcentration membranes to effectively exclude and preconcentrate aptamers without inducing concentration polarization and without localized pH extremes that might interfere with integrated separations analysis. Adding modest amounts of acrylamido buffering components into the polymer matrix to impart a slightly negative charge in the membrane enabled successful binding assays following highly efficient preconcentration of aptamer via both size and charge.

Aptamers were first synthesized 20 years ago and are still developing as diagnostic agents. We anticipate continued progress in aptamer design and synthesis and further incorporation of aptamers into commercial systems due to the inherent benefits of aptamers over conventional antibodies. Combined with the high sensitivity, small analyte consumption, low power requirements, and ease of use of our device, this technology can rapidly provide clinically relevant results in challenging resource-limited environments, a vast improvement over many current models. The use of aptamers in integrated on-chip electrophoretic molecular recognition assays provides a powerful new avenue for on-chip diagnostics.

ACKNOWLEDGMENT

A.H.H. and G.J.S. contributed equally to this manuscript. Aptamer evaluations were supported by NASA SBIR Contract No. NNX10CA98C. The microfluidic platform development and integrated diagnostic system was partially supported by the National Institute of Allergies and Infectious Disease Grant U01A1075441 and by Sandia Lab Directed Research and Development Award 09-0856. This research was partially performed under an appointment to the Department of Homeland Security (DHS) Scholarship and Fellowship Program, administered by the Oak Ridge Institute for Science and Education (ORISE) through an interagency agreement between the U.S. Department of Energy (DOE) and DHS. ORISE is managed by Oak Ridge Associated Universities (ORAU) under DOE Contract No. DE-AC05-06OR23100. All opinions expressed in this paper are the authors' and do not necessarily reflect the policies and views of DHS, DOE, or ORAU/ORISE. Sandia is a multiprogram laboratory operated by Sandia Corp., a Lockheed Martin Co., for the United States Department of Energy under Contract DE-AC0494AL85000.

SUPPORTING INFORMATION AVAILABLE

Additional information as noted in text. This material is available free of charge via the Internet at http://pubs.acs.org.

Received for review April 27, 2010. Accepted September 19, 2010.

AC101106M